Available online at www.sciencedirect.com
SCIENCE DIRECT
Journal of Magnetic Resonance 180 (2006) 280–285
JMR Journal of Magnetic Resonance
www.elsevier.com/locate/jmr

Mapping the intracellular fraction of water by varying the gradient pulse length in *q*-space diffusion MRI

Carin Malmborg [a], Martin Sjöbeck [c], Sara Brockstedt [b], Elisabeth Englund [c], Olle Söderman [a], Daniel Topgaard [a,*]

[a] *Department of Physical Chemistry 1, Lund University, P.O. Box 124, SE-221 00 Lund, Sweden*
[b] *Department of Medical Radiation Physics, Lund University, Sweden*
[c] *Department of Pathology, Lund University, Sweden*

Received 6 December 2005; revised 16 February 2006
Available online 29 March 2006

Abstract

Finite gradient pulse lengths are traditionally considered a nuisance in *q*-space diffusion NMR and MRI, since the simple Fourier relation between the acquired signal and the displacement probability is invalidated. Increasing the value of the pulse length leads to an apparently smaller value of the estimated compartment size. We propose that *q*-space data at different gradient pulse lengths, but with the same effective diffusion time, can be used to identify and quantify components with free or restricted diffusion from multiexponential echo decay curves obtained on cellular systems. The method is demonstrated with experiments on excised human brain white matter and a series of model systems with well-defined free, restricted, and combined free and restricted diffusion behavior. Time-resolved diffusion MRI experiments are used to map the spatial distribution of the intracellular fraction in a yeast cell suspension during sedimentation, and observe the disappearance of this fraction after a heat treatment.

Keywords: PGSE; Pulsed field gradient; Tissue; SGP; Imaging

1. Introduction

Diffusion NMR and MRI experiments performed on water in biological tissues almost invariably display non-exponential signal decays. This is also true for the clinically important case of water diffusion in brain tissues [1]. Because of the complexity of tissue, assignment of the various exponentials is far from trivial [2,3]. A proper assignment is, of course, essential for the further development of diffusion MRI as a tool for diagnosis of, e.g., ischemic stroke, brain tumors, multiple sclerosis, and Alzheimer's disease [4].

Non-exponential echo decays could result from multicomponent free (Gaussian) diffusion, restricted (non-Gaussian) diffusion, or a combination of both. Free or restricted diffusion is traditionally distinguished by performing the diffusion experiment at different values of the effective diffusion time t_d. Free diffusion yields an apparent diffusion coefficient D that is independent of t_d, while restricted diffusion is verified by a root-mean-square displacement Z_{rms} independent of t_d [5–7]. The finite permeability of the cell membrane makes a clear-cut distinction of free and restricted components difficult when using data obtained at different values of t_d.

In the short-gradient-pulse (SGP) limit, the diffusion propagator can be obtained through an inverse Fourier transform of the diffusion NMR signal acquired as a function of the wave vector q defined by the strength and duration of the magnetic field gradient pulses [5]. The size and shape of the confining geometry can be estimated from the propagator in the limit of long t_d [7,8]. The breakdown of the SGP limit has been studied in some detail using a variety of approaches [9–11]. Increasing the value of the

* Corresponding author. Fax: +46 46 2224413.
E-mail address: daniel.topgaard@fkem1.lu.se (D. Topgaard).

1090-7807/$ - see front matter © 2006 Elsevier Inc. All rights reserved.
doi:10.1016/j.jmr.2006.03.005

pulse length δ results in an apparent shrinkage of the pore. The pulse length is smaller than t_d, often by an order of magnitude, and is therefore less affected by molecular exchange between the various compartments.

In this paper, we show how restricted components in multiexponential echo decay curves can be identified by varying δ. The ratio between the Gaussian and non-Gaussian components is a measure of the ratio between the intra- and extracellular compartments. Such an estimate could verify or disprove the various mechanisms proposed for ischemic stroke [4,12,13]. The approach is demonstrated on a series of systems with increasing complexity: a polymer solution with multicomponent Gaussian diffusion, a highly concentrated water-in-oil emulsion with both Gaussian and restricted species, a yeast cell system with water located both inside and between the cells, and a sample of excised human brain white matter.

2. Theoretical considerations

The basics of the diffusion NMR experiment are described in several textbooks [14,15] and review articles [16–18]. Below follows a short review of the pertinent theory in order to provide a basis for the discussion of the experimental results.

The schematic pulse sequence shown in Fig. 1 relies on two rectangular gradient pulses of strength G and duration δ to encode and decode the positions of the molecules [19]. The time between the onset of the pulses is denoted Δ. The effect of the first gradient pulse is to wrap the x, y-magnetization into a helix with spatial frequency $q = \gamma G\delta/2\pi$, where γ is the magnetogyric ratio. After the second gradient pulse, which unwraps the magnetization helix, the signal is detected. Diffusion on a length scale comparable to, or larger than, q^{-1} during the time between the gradient pulses leads to an attenuation of the detected signal E. In the SGP approximation, the winding and unwinding of the magnetization helix is assumed to take place instantaneously. Neglecting nuclear relaxation processes, E is given by [5]

$$E(q,\Delta) = \int P(Z,\Delta)\exp(i2\pi qZ)\,dZ, \tag{1}$$

where $P(Z,\Delta)$ is the average propagator, i.e., the probability density that the spins move the distance Z during the time Δ. According to Eq. (1) there is a Fourier relation between the measured signal and the displacement probability. From a series expansion of Eq. (1) it can be shown that the initial, low-q, decay of E is given by

$$\lim_{q\to 0} E(q,\Delta) = \exp(-2\pi^2 q^2 Z_{rms}^2), \tag{2}$$

where Z_{rms} is the root-mean-square displacement during the time Δ, i.e., the width of the distribution $P(Z,\Delta)$. As long as the conditions for the SGP approximation are fulfilled, Eq. (2) is valid irrespective of the actual shape of $P(Z,\Delta)$. For Gaussian diffusion the effect of the gradient pulse length can be taken into account by introducing an effective diffusion time $t_d = \Delta - \delta/3$. If this correction is attempted for molecules experiencing restricted diffusion on the time scale of δ, the estimated value of Z_{rms} will decrease with increasing δ [10,20]. The reason for this decrease can be understood from Fig. 2. The particle is labeled for a position given by the center-of-mass average of the path during the application of the gradient pulse. With infinitely short pulses the particle can be labeled for any position within the pore, even next to the pore wall. As the pulse length is increasing it is less likely that the particle will be labeled for a position close to a pore wall. In the limit of very long pulses the particle will be labeled for the center of the pore since the entire pore space has been sampled during the application of the pulse.

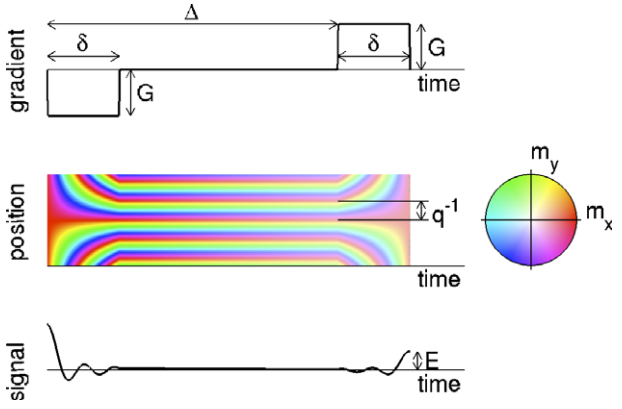

Fig. 1. Schematic of the diffusion NMR pulse sequence. Top panel: gradient modulation scheme with pulse length δ, diffusion time Δ, and gradient strength G indicated. Middle panel: evolution of the transverse magnetization $m_{x,y}$ (color coded according to the unit circle shown to the right). q^{-1} is the wavelength of the magnetization helix. Bottom panel: NMR signal. E is the echo intensity normalized to the value obtained at $G = 0$.

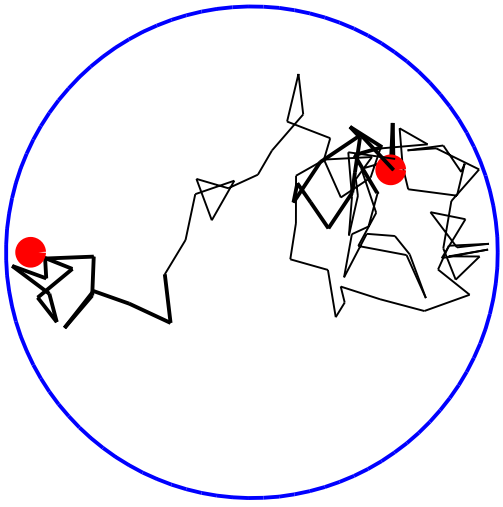

Fig. 2. Trajectory of a particle confined in a pore. The position for which the particle is encoded is given by the center-of-mass average of the path during the application of the gradient pulse (shown with bold lines).

3. Experimental details

3.1. NMR experiments

NMR experiments were performed at 25 °C, unless otherwise stated, on a Bruker DMX-200 spectrometer operating at 200.13 MHz proton resonance frequency. Pulsed field gradients were generated by a Bruker DIFF-25 gradient probe driven by a BAFPA-40 current supply. This setup can produce magnetic field gradients with a maximum strength of 9.6 T/m in the z-direction. Diffusion was measured with the pulsed field gradient stimulated echo pulse sequence [21]. Spatial resolution in the z-direction was achieved by applying a 48 mT/m read gradient during signal direction. Variable-δ experiments were performed with constant separation between the RF pulses and constant $t_d = \Delta - \delta/3$. The gradient strength was adjusted to keep the q-values independent of the value of δ. Explicit values of t_d and δ are given in the figure captions. Because of the wide distribution of diffusion coefficients in the studied systems the gradients were increased in a geometric sequence in contrast to the customary linear one. With 8 scans and 2 s recycle delay the whole set of spectroscopic experiments was performed in approximately 20 min (polymer, yeast, and brain) or 40 min (emulsion) per sample. The imaging experiments were performed with a spatial resolution of 190 μm and a time resolution of 20 min (including a 10 min waiting time).

3.2. Preparation of samples

The highly concentrated water-in-oil emulsion was prepared by adding a water solution containing a H_2O/D_2O mixture (20 g H_2O in 50 ml solution) and 0.2 M tetramethyl ammonium chloride (TMACl) to an oil/surfactant mixture consisting of heptane (57.5 wt%), lecithin (7.5 wt%), and $C_{12}EO_4$ (35 wt%). The H_2O/D_2O composition was chosen to have a reasonable ratio between the signals of the H_2O and the TMA^+ ions. The water solution was added slowly to the oil phase while shaking on a vortex mixer and, when the emulsion became more viscous, by hand. The final emulsion contained 96 wt% of the water phase. Emulsion stability during the course of the NMR experiments was verified by recording "diffusion diffractograms" [22].

The aqueous polymer solution contained 50 wt% polyethylene glycol (PEG) with molecular weight between 1305 and 1595 g/mol (supplier specification) dissolved in H_2O.

The yeast sample was prepared by suspending ordinary baker's yeast in H_2O and letting the yeast cells sediment in the NMR tube overnight at 4 °C. NMR experiments started after 1 h equilibration at 25 °C. Yeast activity resulted in gas bubble formation in the sediment on the time scale of 12 h. No visible bubble formation occurred during the NMR experiments (20 min). Time-resolved MRI experiments were performed while a sediment was formed from an initially homogeneous yeast cell suspension in a standard 5 mm NMR tube at 4 °C. Heat treatment was performed by raising the temperature within the magnet to 70 °C for 1 h.

A case with clinically and neuropathologically diagnosed vascular dementia and ischemic white matter pathology was chosen for post-mortem NMR measurements. For clinical/neuropathological analysis, the brain was fixed in 6% formaldehyde solution for 6 weeks and later cut in 10 mm whole-brain coronal slices that were sectioned and stained for microscopy. Utilising the 5 mm OD NMR sample tube, a sample from the deep frontal white matter was taken from the cut whole brain and placed in formaldehyde solution. For the NMR experiments the excess formaldehyde solution was removed and the tissue sample was put in an NMR tube. Post-mortem NMR investigations were made with permission from the ethics committee at Lund University (LU 685-01 and LU 926-02).

4. Results and discussion

Experimental results for the highly concentrated emulsion are shown in Fig. 3. This system has been thoroughly

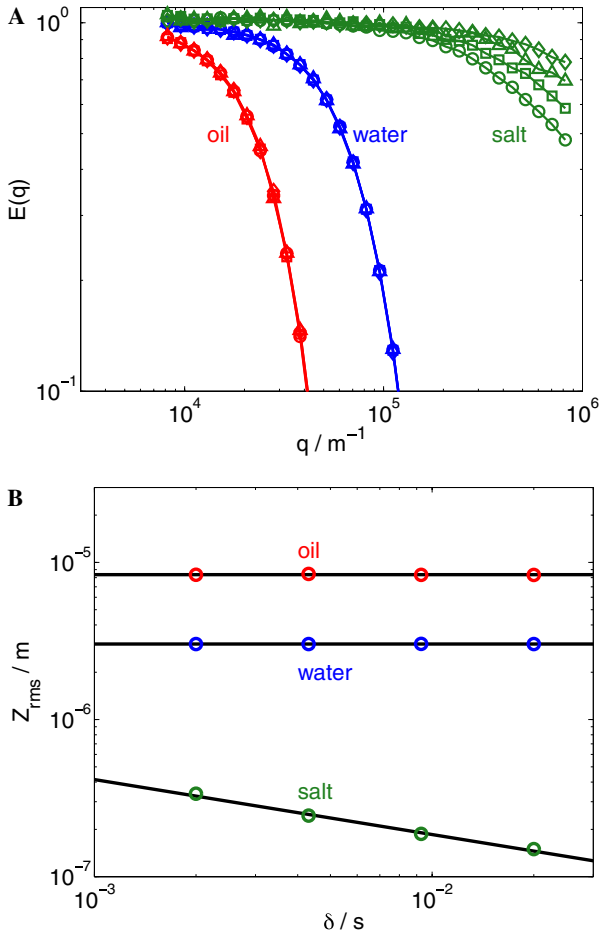

Fig. 3. Effect of finite gradient pulse length for oil (red), water (blue), and salt (green) in a highly concentrated water-in-oil emulsion. (A) Experimental echo intensity E vs. the wave vector q using the parameters $t_d = 40$ ms and $\delta = 2.0$ (circles), 4.3 (squares), 9.3 (triangles), and 20 ms (diamonds). (B) Root-mean-square displacement Z_{rms} vs. pulse length δ evaluated from the initial slope of the data in (A). (For interpretation of the references to color in this figure legend, the reader is referred to the web version of this paper.)

characterized by diffusion NMR methods [20,22–25]. The diffusion of oil, water, and salt can be studied simultaneously since the different species give rise to resolved resonances in the NMR spectrum. The emulsion consists of discrete water droplets in a continuous oil phase. The droplet radius is estimated to about 1 μm from "diffusion diffractogram" coherence peaks (not shown) [23]. Due to the high volume fraction of water, in excess of 90%, the thickness of the oil film separating adjacent droplets is only about 10 nm. The long-range diffusion of water-soluble substances depends on the ability of the substance to penetrate through the oil film. Water has a small, but finite, oil solubility, while charged species, like the TMA^+ ions studied here, are practically insoluble in the oil. Consequently, the long-range water diffusion is reduced a factor ~10 from the bulk value [25], while the salt displacement is limited by the droplet size. The reduction of the oil diffusion from the bulk value is related to the tortuosity of the pore space in which the oil is located.

As shown in Fig. 3A the signals from the water and the oil are independent of the value of δ indicating Gaussian diffusion. The water signal displays a coherence peak outside the scale of the figure. The influence of δ on this peak is studied in [20]. Increasing δ leads to a shift of the decay of the salt signal towards higher q-values indicating an apparently smaller value of Z_{rms}. Fig. 3B displays Z_{rms} evaluated by fitting Eq. (2) to the data in Fig. 3A using data points fulfilling $E > 0.8$. The values for the oil and the water are constant while the value for the salt is decreasing with δ. For spherical pores with radius r the limiting value of Z_{rms} equals $(2/5)^{1/2}r \approx 0.63r$ [14]. A crude extrapolation of the data for the salt indicates that it is necessary to use pulse lengths below 0.3 ms to measure the correct value of Z_{rms} for spherical pores with 1 μm radius. It is quite likely that the exact dependence of the apparent Z_{rms} on δ could yield useful information about the pore geometry in the same manner as time-dependent apparent diffusion coefficients give the surface-to-volume ratio of the pore space [26]. This subject is outside the scope of the current paper, but is well worth future studies.

The data in Fig. 3 clearly show that by performing experiments with different δ, but constant q-range, t_d, and relaxation weighting, it can be determined whether the diffusion of a substance obeys Gaussian statistics. The aim of this work is to identify and quantify the amount of a single substance located in different compartments, the morphology of which gives rise to different diffusion statistics. In this case there is no spectroscopic resolution of the various components contributing to the multiexponential echo decay. Extracting the various exponentials from a featureless decay curve through either numerical Laplace inversion or multiexponential curve fitting is a difficult problem that suffers from non-uniqueness of the solution [27]. An experiment that gives easily interpretable information without requiring an inversion of the decay curve would be highly useful. For experiments on water in cellular systems the initial, low-q, part of the decay curve originates from the extracellular space with fast diffusion, and the final, high-q, part of the decay results from water confined in the cells [28]. Neglecting molecular exchange and differences in relaxation, the fraction of water located inside the cells can then simply be estimated from the point where the decay curves measured at different values of δ start to deviate. This fact is illustrated in Fig. 4 showing experiments performed on three different samples exhibiting multiexponential signal decays, but with different diffusion statistics. Consequently the signal decays are affected differently by the value of δ.

The data for the aqueous polymer solution in Fig. 4A contains contributions from both water and slowly diffusing polymer. The polymer diffusion depends on the molecular size [29] and is further reduced by chain entanglement since the polymer concentration is well above the value at which the individual polymer molecules start to overlap. The data for different δ collapse on a single curve verifying Gaussian diffusion of all components, both fast and slow.

The situation is rather different for the yeast cells in Fig. 4B. In this case there is an initial Gaussian decay corresponding to the free water outside the cells, and a final non-Gaussian decay originating from the restricted intracellular component [6]. The curves start to deviate at $E \approx 0.35$, which can be interpreted as a relaxation-weighted intracellular fraction P_{int} of 35%. Work is in progress to quantify the relaxation effect by performing diffusion–relaxation correlation experiments [30].

In Fig. 4C the data for the brain tissue is shown. Also in this case there is an initial Gaussian and a final non-Gaussian decay. This is in accord with the recent observation by Nossin-Manor et al. [31] that longer values of δ lead to a larger signal from the slow-diffusion component. The border between the two types of behavior is located at about $E = 0.5$, but the exact location is less well defined than for the yeast sample. This is the result of the local anisotropy of the structure. Whereas the yeast cells are roughly spherical, nerve fibers are cylindrical. The amount of restricted water depends on the direction of the applied gradients. When the gradients are oriented in parallel with the fiber direction all water appears to be free. The true intracellular fraction can only be determined from measurements perpendicular to the fibers. In a macroscopic sample there is a distribution of fiber orientations, thus smearing the transition between Gaussian and non-Gaussian decay as observed in Fig. 4C. The NMR equipment used here only allows for measurements in one direction. Characterizing the anisotropy of the effect of variable δ is important for studies of nerve fiber orientation and will be the subject of future studies. It is quite likely that adding the information from the effect of δ to current 3D q-space experiments [28] would improve the accuracy of the estimation of the direction and distribution of nerve fiber orientations.

The results of the diffusion MRI experiments are shown in Fig. 5. The intracellular fraction P_{int} was estimated for

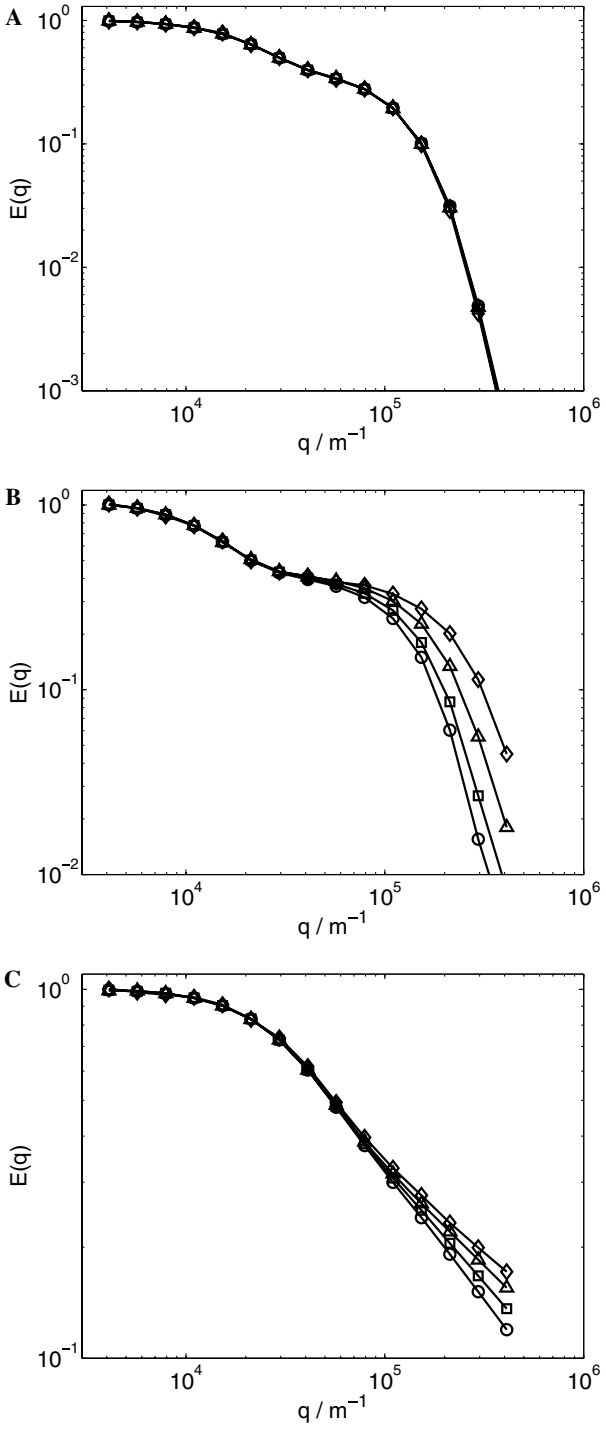

Fig. 4. Experimental echo intensity E vs. the wave vector q for a polymer solution (A), yeast cells (B), and brain white matter (C). The following parameters were used: $t_d = 100$ ms and $\delta = 1.0$ (circles), 2.2 (squares), 4.6 (triangles), and 10 ms (diamonds). The fraction intracellular water P_{int} is given by the value of E where data obtained at different values of δ start to deviate.

each pixel by comparing $E(q)$ for two values of δ (0.5 and 5 ms). A simple algorithm was written to identify P_{int} as the largest value of $E(q, \delta = 5\text{ ms})$ where the ratio $E(q, \delta = 5\text{ ms})/E(q, \delta = 0.5\text{ ms})$ exceeded 1.2. One-dimensional maps of P_{int} are shown in Fig. 5A for the polymer

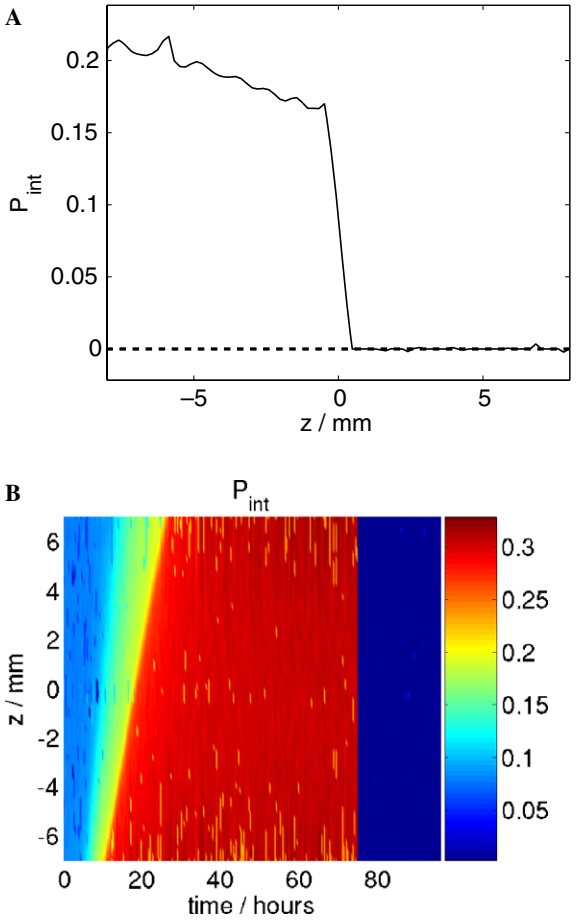

Fig. 5. Mapping the fraction intracellular water P_{int} using a diffusion MRI sequence with $t_d = 50$ ms and $\delta = 0.5$ and 5 ms. (A) P_{int} as a function of position z for a yeast cell sediment (solid) and a polymer solution (dashed). (B) P_{int} as a function of z and time for a yeast cell suspension during sedimentation. Heat treatment was applied after 75 h.

solution and the yeast sediment. Since the diffusion is Gaussian for all components in the polymer solution, $E(q)$ for the two values of δ coincide, cf. Fig. 4A, and the algorithm returns $P_{int} = 0$ for all values of z. The top surface of the yeast sediment was located at $z = 0$. Although the diffusion coefficients are similar for the polymer and the yeast systems, the non-Gaussian behavior of the intracellular water results in a sharp step in P_{int} at $z = 0$. Larger values of P_{int} are obtained further down in the sediment where the cells are more tightly packed.

Time-resolved P_{int}-profiles for a yeast cell suspension in a standard 5 mm NMR tube are displayed in Fig. 5B. The sample is initially homogeneous with $P_{int} = 8\%$. At times between 10 and 30 h a sediment of cells gradually fills the part of the tube located in the active volume of the RF coil. As time goes on the sediment becomes more packed, finally reaching $P_{int} = 32\%$. After 75 h, the temperature within the magnet is temporarily raised to 70 °C. This "pasteurization" of the sample leads to a disruption of the cell membranes and the complete disappearance of the intracellular fraction. Thus, P_{int} estimated from diffusion NMR/MRI with variable δ could be a sensitive measure for tissue integrity.

5. Conclusions

NMR diffusometry experiments performed with varying gradient pulse length, all other relevant parameters being constant, are capable of identifying Gaussian and non-Gaussian components in multiexponential echo decay curves. For tissue such measurements can be used to estimate the fraction intracellular water and, for anisotropic structures, the direction of the cells. This study also shows the great utility of well-defined colloidal model systems when designing new MR methods for clinical applications.

Acknowledgments

This work is supported by the Swedish Research Council (VR) and the Organon Foundation.

References

[1] Y. Assaf, Y. Cohen, Non-mono-exponential attenuation of water and N-acetyl aspartate signals due to diffusion in brain tissue, J. Magn. Reson. 131 (1998) 69–85.
[2] Y. Assaf, Y. Cohen, Structural information in neuronal tissue as revealed by q-space diffusion NMR spectroscopy of metabolites in bovine optic nerve, NMR Biomed. 12 (1999) 335–344.
[3] Y. Assaf, Y. Cohen, Assignment of the water slow-diffusing component in the central nervous system using *q*-space diffusion MRS: implications for fiber tract imaging, Magn. Reson. Med. 43 (2000) 191–199.
[4] D. Le Bihan, Looking into the functional architecture of the brain with diffusion MRI, Nat. Rev. Neurosci. 4 (2003) 469–480.
[5] J. Kärger, W. Heink, The propagator representation of molecular transport in microporous crystallites, J. Magn. Reson. 51 (1983) 1–7.
[6] D.G. Cory, A.N. Garroway, Measurement of translational displacement probabilities by NMR—an indicator of compartmentation, Magn. Reson. Med. 14 (1990) 435–444.
[7] D. Topgaard, O. Söderman, Experimental determination of pore size and shape using *q*-space NMR microscopy in the long diffusion-time limit, Magn. Reson. Imaging 21 (2003) 69–76.
[8] P.W. Kuchel, A. Coy, P. Stilbs, NMR "diffusion-diffraction" of water revealing alignment of erythrocytes in a magnetic field and their dimensions and membrane transport characteristics, Magn. Reson. Med. 37 (1997) 637–643.
[9] P. Linse, O. Söderman, The validity of the short-gradient-pulse approximation in NMR studies of restricted diffusion, simulations of molecules diffusing between planes, in cylinders and spheres, J. Magn. Reson. A 116 (1995) 77–86.
[10] P.P. Mitra, B.I. Halperin, Effects of finite gradient-pulse widths in pulsed-field-gradient diffusion measurements, J. Magn. Reson. A 113 (1995) 94–101.
[11] P.T. Callaghan, A simple matrix formalism for spin echo analysis of restricted diffusion under generalized gradient waveforms, J. Magn. Reson. 129 (1997) 74–84.
[12] M.E. Moseley, Y. Cohen, J. Mintorovitch, L. Chileuitt, H. Shimizu, J. Kucharczyk, M.F. Wendland, P.R. Weinstein, Early detection of regional cerebral-ischemia in cats—comparison of diffusion-weighted and T2-weighted MRI and spectroscopy, Magn. Reson. Med. 14 (1990) 330–346.
[13] C.H. Sotak, Nuclear magnetic resonance (NMR) measurements of the apparent diffusion coefficient (ADC) of tissue water and its relationship to cell volume changes in pathological states, Neurochem. Int. 45 (2004) 569–582.
[14] P.T. Callaghan, Principles of Nuclear Magnetic Resonance Microscopy, Clarendon Press, Oxford, 1991.
[15] R. Kimmich, NMR: Tomography, Diffusometry, Relaxometry, Springer-Verlag, Berlin, 1997.
[16] P. Stilbs, Fourier transform pulsed-gradient spin-echo studies of molecular diffusion, Prog. Nucl. Magn. Reson. Spectrosc. 19 (1987) 1–45.
[17] W.S. Price, Pulsed-field gradient nuclear magnetic resonance as a tool for studying translational diffusion: part 1. Basic theory, Concepts Magn. Reson. 9 (1997) 299–336.
[18] F. Stallmach, J. Kärger, The potentials of pulsed field gradient NMR for investigation of porous media, Adsorption 5 (1999) 117–133.
[19] E.O. Stejskal, J.E. Tanner, Spin diffusion measurements: spin echoes in the presence of a time-dependent field gradient, J. Chem. Phys. 42 (1965) 288–292.
[20] C. Malmborg, D. Topgaard, O. Söderman, NMR diffusometry and the short gradient pulse approximation, J. Magn. Reson. 169 (2004) 85–91.
[21] J.E. Tanner, Use of stimulated echo in NMR diffusion studies, J. Chem. Phys. 52 (1970) 2523–2526.
[22] C. Malmborg, D. Topgaard, O. Söderman, Diffusion in an inhomogeneous system: NMR studies of diffusion in highly concentrated emulsions, J. Colloid Interface Sci. 263 (2003) 270–276.
[23] B. Balinov, O. Söderman, J.C. Ravey, Diffraction-like effects observed in the PGSE experiment when applied to a highly concentrated water/oil emulsion, J. Phys. Chem. 98 (1994) 393–395.
[24] B. Håkansson, R. Pons, O. Söderman, Structure determination of a highly concentrated W/O emulsion using pulsed-field-gradient spin-echo nuclear magnetic resonance "diffusion diffractograms," Langmuir 15 (1999) 988–991.
[25] D. Topgaard, C. Malmborg, O. Söderman, Restricted self-diffusion of water in a highly concentrated W/O emulsion studied using modulated gradient spin-echo NMR, J. Magn. Reson. 156 (2002) 195–201.
[26] P.P. Mitra, P.B. Sen, L.M. Schwartz, Short-time behavior of the diffusion coefficient as a geometrical probe of porous media, Phys. Rev. B 47 (1993) 8565–8574.
[27] K.P. Whittal, A.L. MacKay, Quantitative interpretation of NMR relaxation data, J. Magn. Reson. 84 (1989) 134–152.
[28] Y. Assaf, R.Z. Freidlin, G.K. Rohde, P.J. Basser, New modeling and experimental framework to characterize hindered and restricted water diffusion in brain white matter, Magn. Reson. Med. 52 (2004) 965–978.
[29] B. Håkansson, M. Nydén, O. Söderman, The influence of polymer molecular-weight distributions on pulsed field gradient nuclear magnetic resonance self-diffusion, Colloid Polym. Sci. 278 (2000) 399–405.
[30] M. Hürlimann, L. Venkataramanan, Quantitative measurements of two-dimensional distribution functions of diffusion and relaxation in grossly in homogenous fields, J. Magn. Reson. 157 (2002) 31–42.
[31] R. Nossin-Manor, R. Duvedevani, Y. Cohen, Effect of experimental parameters on high b-value q-space MR images of excised rat spinal cord, Magn. Reson. Med. 54 (2005) 96–104.